Available online at www.sciencedirect.com
SCIENCE DIRECT®
Journal of Catalysis 222 (2004) 323–337
JOURNAL OF CATALYSIS
www.elsevier.com/locate/jcat

Effects of zeolite pore sizes on the mechanism and selectivity of xylene disproportionation—a DFT study

Thomas Demuth,[a] Pascal Raybaud,[a,*] Sylvie Lacombe,[b] and Hervé Toulhoat[c]

[a] *Institut Français du Pétrole, Direction Chimie et Physico-Chimie Appliquées, 1 & 4 avenue de Bois-Préau, 92852 Rueil-Malmaison cedex, France*
[b] *IFP, Division Catalyse et Séparation, BP n° 3-69390, Vernaison, France*
[c] *Institut Français du Pétrole, Direction Scientifique, 1 & 4 avenue de Bois-Préau, 92852 Rueil-Malmaison cedex, France*

Received 23 July 2003; revised 17 October 2003; accepted 21 October 2003

Abstract

The disproportionation reaction of xylenes, catalyzed by acidic zeolites, is investigated by means of periodic ab initio calculations. Two relevant 10- and 12-membered ring (MR) frameworks are chosen: theta-1 (TON) and mordenite (MOR). As a first step, two bimolecular mechanisms proposed for this reaction are investigated: the first one is assumed to occur through a one-step methyl shift and involves a highly unstable methyl cation as a transition state. The second and energetically favored mechanism implies the formation of a benzylic-like carbocation, subsequently converted into a trimethyldiphenylmethane, also called DPM intermediate. The energetics of this reaction path are mainly governed by the different sterical constraints induced by the 10-MR or 12-MR zeolites on the DPM intermediates. Therefore, the relative stability of the DPM inside the pores appears as the key parameter for understanding the selectivity observed experimentally.

Keywords: Isomerization; Disproportionation; Xylene; Zeolite; Ab initio; Molecular modeling; Selectivity; Pore sizes

1. Introduction

The catalytic conversion of aromatic molecules via transalkylation or isomerization is a very important process in the petrochemical industrial [1]. For this purpose, exclusively zeolite catalysts are industrially used nowadays. They offer numerous advantages as compared to the traditional Friedel–Crafts catalysts; e.g., they allow stereochemical control over the reaction, and they are more environmental friendly. Indeed, zeolites are successfully used for hydrocarbon transformations since a high selectivity for the desired product can be achieved. The shape selectivity originates from their microporous structure and depending on the zeolite pore size or topology, various product patterns are observed [2].

Xylene isomerization is a significant step in the synthesis of the *para* isomer, an important raw material for fibers, films, and packing materials [3,4]. Over acidic catalysts, this transformation occurs mainly by an intramolecular reaction involving a carbenium ion as an intermediate, which further undergoes a 1,2 methyl shift. Hence, *meta*-xylene is converted into *para* and *ortho*, and vice versa. However, this mechanism does not permit the direct interconversion of *para*- to *ortho*-xylene, as observed experimentally [5]. An alternative pathway, proceeding via a bimolecular reaction, is the disproportionation of two xylenes with a trimethyldiphenylmethane intermediate (called DPM in this paper), yielding toluene and trimethylbenzene (TMB) as products. The disproportionation is followed by a transalkylation between TMB and the reactant, leading to a mixture of xylenes and TMBs. The presence of this bimolecular pathway for isomerization on large-pore zeolites was confirmed by numerous experimental studies [5,6]. For the disproportionation reaction mechanism itself, two different scenarii are proposed in the literature, either it is mediated by a methyl shift reaction or it occurs via the formation of a DPM-like intermediate [3,5]. Isotope-labeling experiments during toluene disproportionation provided evidence that the DPM-mediated pathway is important even in the small channels of ZSM-5 [7]. The disproportionation reaction of alkylated xylenes is also frequently used as a catalytic test reaction for determining the topology and dimension of intracrystalline void space of molecular sieves [8].

* Corresponding author.
E-mail address: pascal.raybaud@ifp.fr (P. Raybaud).

0021-9517/$ – see front matter
doi:10.1016/j.jcat.2003.10.017

Martens et al. [9] studied the conversion of *m*-xylene in various 10- and 12-MR zeolites. First, they found that the isomerization/disproportionation (i/d) selectivity was very high for 10-MR zeolites like ZSM-5 or ZSM-48, whereas a much lower ratio was observed for 12-MR zeolites, like MOR or ZSM-12. However, for the 12-MR zeolites, no obvious correlation between the (i/d) ratio and the pore-size diameter was found. The high selectivity for isomerization in 10-MR zeolites was attributed to the bimolecular nature of the disproportionation reaction which would be sterically unfavored in small pore sizes. Additionally, they observed that the distribution among the TMB products is mainly dominated by the 1,2,4 isomer, whatever the pore-size geometry or dimension of the studied zeolites may be. More precisely, the selectivity in 1,2,4-TMB is 100% for 10-MR zeolites, whereas a significant decrease was found for larger 12-MR structures, facilitating the formation of 1,3,5- and 1,2,3-TMB. Similar results were obtained more recently by Adair et al. [10] and Jones et al. [11]. Martens et al. proposed to explain this feature by the size of the different transition state complexes or intermediates, which accommodate more or less easily in the zeolitic intracrystalline void spaces. However, no rigorous demonstration has been provided up to now.

Although an acid-catalyzed disproportionation mechanism of alkylated aromatics has been the subject of theoretical studies [12,13], to our knowledge, the energetic properties and local geometrical arrangement of the various adsorbed DPM isomers in relevant zeolitic void spaces remain to be explored. Thus, the main objective of the present paper is to evaluate pore-size effects in 10- and 12-MR frameworks on the reaction mechanism of the *m*-xylene disproportionation, and to understand the experimental (i/d) selectivity observed as well as the TMB product distribution. For this purpose, we will first present and investigate the two proposed reaction pathways in the 10-MR framework of theta-1 (TON), and afterward show how the energy profile is modified, when occurring in a 12-MR environment, as the one of mordenite (MOR). The second part of the work is devoted to the interpretation of the selectivity observed, and to establish a correlation with the destabilization energy for the adsorbed DPM intermediates.

2. Methods

2.1. Total energy calculations

Ab initio total energy calculations are performed using the Vienna ab initio simulation package VASP [14,15]. VASP performs an iterative solution of the Kohn–Sham equations of density–functional theory, based on the minimization of the norm of the residual vector to each eigenstate and an efficient charge-density mixing. For the exchange-correlation functional, gradient-corrected functionals in the form of the generalized gradient approximation (GGA) of Perdew and Wang 91 are used [16]. The calculations are performed in a plane-wave basis set, using the projector-augmented wave (PAW) method [17,18], and a plane-wave cutoff of 400 eV. Due to the large unit cell of zeolites, it is legitimate to restrict the Brillouin-zone sampling to the Γ-point, using a modest smearing of the eigenvalues to improve total energy convergence. For structural relaxation a conjugate-gradient algorithm is chosen. Except for the cell volume, which is fixed to the experimental value, all lattice constants and all internal parameters are allowed to relax. The SCF electronic convergence is fixed at 0.1 meV/cell, while the geometry optimization is ensured to have converged when forces acting upon ions are less than 0.07 eV/Å. For calculating reaction energy barriers, the nudged elastic band method is used [19]. In this method, a string of images of the system is created and connected together with springs. An optimization algorithm is then applied, relaxing the images downward the minimum energy path, constraining that they are only allowed to move in the direction perpendicular to the current hypertangent. The image exhibiting a maximum in energy (transition state) is afterward optimized separately, till the forces acting on the ions are less than 0.05 eV/Å. The system that is finally obtained corresponds to an estimate of the transition-state complex (i.e., maximum energy with forces close to zero). All transition-state structures are subjected to a frequency analysis to verify the presence of only one imaginary frequency by a numerical evaluation of the force constants.

It is well known that within DFT calculations, van der Waals (vdW) contributions to the interaction energy are generally not correctly taken into account [20]. Moreover, the adsorption between alkylated aromatics and the zeolite framework is dominated by dispersive interactions [21]. Thus, for calculating reliable absolute values of adsorption energies, it is required that vdW interactions be included. For this purpose, we calculate the vdW contributions acting on the final relaxed DFT geometries by means of the DISCOVER module [22] and the COMPASS force field [22,23] within the Cerius^2 software suite [22]. In a previous study [24], the accuracy of this force field was successfully proven for studying adsorption phenomena of hydrocarbon molecules within zeolitic systems.

2.2. Zeolite structures of TON and MOR

The TON and MOR frameworks are chosen to study the disproportionation reaction of *m*-xylene since they exhibit channels formed by 10- and 12-MR channels, respectively. Especially mordenite is frequently used as catalyst in the petrochemical industry for hydrocarbon transformation reactions like isomerization or alkylation [25].

For TON, as represented by ZSM-22 within this study, the main 10-membered ring channel, running parallel to the [001] direction, measures 5.5 × 4.5 Å, and has a framework consisting of 5, 6, and 10 rings [26]. The structure includes ferrierite sheets of the type also found in ZSM-5 and ZSM-

11 and sheets of 6 rings. However, the small channels do not allow molecules to enter or diffuse and, thus, they are not considered as pores. Purely siliceous TON crystallizes in the orthorhombic space group *Cmcm* with lattice constants $a = 13.86$ Å, $b = 17.41$ Å, and $c = 5.04$ Å. Despite the fact that it is necessary to use as supercell a tripled primitive monocline unit cell along the c axis, so as to avoid artificial adsorbate–adsorbate interactions between neighboring images, the total number of atoms ($N_{at} = 108$) in the supercell remains reasonable for performing DFT calculations based on periodic boundary conditions. The optimized lattice constants for this cell are $a = b = 11.17$ Å, $c = 15.012$ Å, $\alpha = 76.72°$, $\beta = 90.12°$, and $\gamma = 89.98°$. One acid site per supercell is considered, corresponding to a Si/Al ratio of 35.

Two types of different cavities are present in the crystal structure of mordenite: (i) a main elliptical channel (measuring 6.7×7.9 Å), circumscribed by 12-membered rings and parallel to the c axis, (ii) smaller channels surrounded by 8-membered rings running along the b axis and measuring 2.6×5.7 Å. Since these narrower channels allow for a diffusion of only small molecules, they are referred to as "small side pockets" that can be entered only from the main channel, but do not provide a connection between adjacent channels. The orthorhombic unit cell of mordenite has the lattice parameters $a = 18.09$ Å, $b = 20.52$ Å, and $c = 7.52$ Å (for further details see [27]). The optimization of the structure yields lattice parameters of $a = b = 13.63$ Å, $c = 15.11$ Å, $\alpha = 96.74°$, $\beta = 90.07°$, and $\gamma = 90.02°$. For the same reasons as for TON a supercell was constructed doubling the unit cell along the c axis. The total number of atoms is 144 with a Si/Al ratio of 47.

3. Results

Traditionally, two pathways are proposed in the literature: either a one-step mechanism via a methyl-shift reaction or a pathway involving the formation of benzylic carbocations, and a diphenylmethane-like intermediate. In the first three sections, we study in detail these two reaction pathways in TON. Then, Section 3.4 is devoted to the MOR case. For Sections 3.2 to 3.4, we focus on the mechanism involving the formation of the 2,4-dimethyl-1-(3-methylbenzyl)benzene (2,4-DPM) and leading to 1,2,4-TMB. Finally, Section 3.5 attempts to give an interpretation of the observed selectivities by comparing the stability of all relevant DPM-like intermediates involved in the xylene disproportionation.

3.1. Methyl-shift pathway

The first reaction scheme is depicted in Fig. 1. In the initial reaction step, the acidic proton activates the physisorbed xylene molecule at the C1 atom (with respect to the methyl group). Consequently, this leads to the formation of a benzenium carbocation intermediate, stabilized by the electrostatic field of the anionic zeolite framework (note that upon protonation the aromaticity of the xylene molecule is reduced). Subsequently, the cleavage of the C1–C2 bond between the methyl group and the fourfold coordinated carbon of the aromatic ring results in the formation of a methyl cation. In the transition state geometry, the methyl ion is located in-between the two aromatic molecules (one toluene and one xylene). Subsequently, the CH_3^+ ion reconnects to the second xylene via a new C2–C3 bond formation. Hence, the product configuration of the transalkylation reaction corresponds to neutral toluene and an activated protonated trimethylbenzene. Finally, the reaction issues in a proton backdonation from the charged TMB to an oxygen atom of the zeolitic framework. For proton transfers to unsaturated hydrocarbon molecules within zeolites, energy barriers are about 60–100 kJ/mol [28]. However, it is important to note that the rate-limiting step of the overall reaction is expected to be the formation of the high-energy methyl carbocation which is known to be energetically the least stable carbocation as compared to primary or secondary carbenium ions. In a recent work, we have investigated the skeletal isomerization reaction of an olefin molecule (2-pentene) catalyzed by acidic TON [28]. It was shown that a pathway mediated by an ethyl shift must be discarded due to its high activation energy as compared with a mechanism only including secondary carbenium ions. Thus, we focus our study on the determination of the transition state involving the formation of the methyl ion and its associated energy barrier. Moreover, in 10-MR zeolites, like TON, the benzenium ion is found to be a stable intermediate along the potential energy surface, as we verified it by a vibrational spectra analysis. The configuration of the reactants before the methyl ion formation corresponds to an activated protonated xylene, the proton being transferred to the C1 atom of the molecule (see Fig. 1) with an increased covalent C1–H bond distance of about 1.14 Å. Due to activation, the C1–C2 bond distance increases to 1.54 Å. The adjacent C1–C bonds of the aromatic ring elongate to 1.45 Å, and the next neighboring C–C distances reduce to 1.37 Å in accordance to the bond order conservation law [29]. The methyl group next to the protonated carbon tilts out by nearly 21° with respect to the plane of the aromatic ring. The optimized transition state configuration is shown in Fig. 2. The newly created methyl ion lies in a position between the two molecules with a slightly smaller C1–C2 distance of 2.70 Å than the C2–C3 distance of 2.77 Å. Due to the sp^2 hybridization of C2, the methyl ion is planar with an average C–H distance of 1.08 Å and intramolecular H–C2–H angles close to 120°. Additionally, one observes a tilting of about 6° for the two hydrogens connected to the C1 and C3 atoms. The product configuration shows finally a neutral toluene and a protonated 1,2,4-trimethylbenzene. The largest structural change concerning the cationic species involves the hydrogen atom bonded to C3. The C3–H bond length increases to 1.15 Å, and the hydrogen atom tilts out strongly by 103° with respect to the aromatic ring. The smallest molecule-zeolite distance

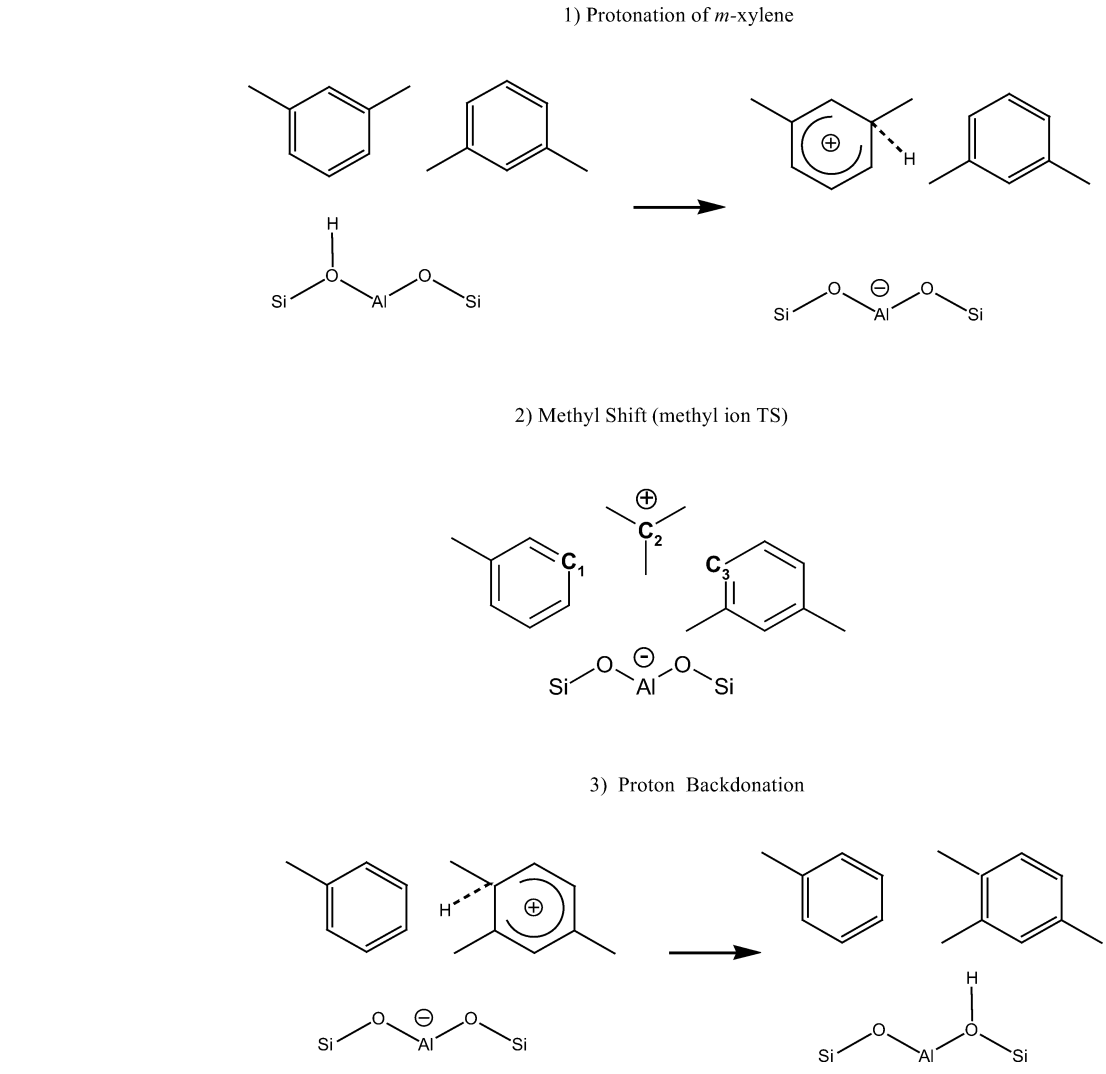

Fig. 1. Reaction mechanism of xylene disproportionation catalyzed by acidic zeolites via a methyl shift.

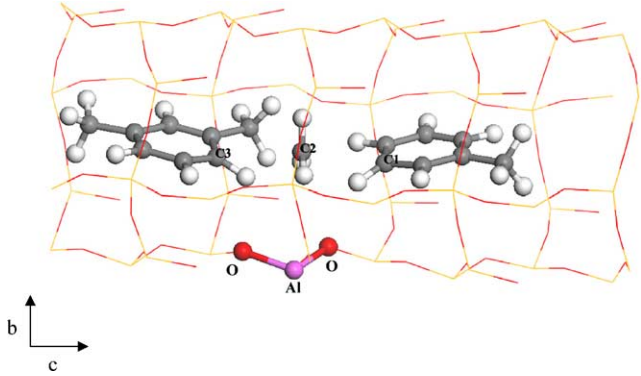

Fig. 2. Transition state geometry for the disproportionation reaction via a methyl shift.

of about 1.95 Å is found between this hydrogen and the oxygen to which the proton will be finally backtransferred.

The reaction energy diagram for the formation step of the methyl ion in TON is depicted in Fig. 3. With respect to the initial configuration (corresponding to the activated xylene), the activation energy is estimated at 166 kJ/mol. When calculated with respect to two xylene molecules adsorbed at acidic ZSM-22, a similar value for the barrier is found because the neutral and activated complexes exhibit a very small energy difference (less than 5 kJ/mol). Moreover, it is seen that the reaction is exothermic by −46 kJ/mol, indicating a higher degree of stabilization for the protonated TMB than for the protonated xylene. The reason for the large barrier originates from the formation of the high-energy methyl ion. Rozanska et al. [12] studied the disproportionation reaction of toluene and benzene in acidic mordenite with the same theoretical methodology. For the direct transalkylation route via a methyl shift, they found a barrier of 180 kJ/mol, with respect to the two physisorbed aromatic molecules. The transition-state geometry in that case exhibited also a methyl ion, similarly sandwiched between the two aromatic molecules. However, due to the larger void space available in the 12-MR of mordenite and due to the lack of additional methyl groups, both aromatic molecules were found in an upright position, with their aromatic planes orthogonal to the

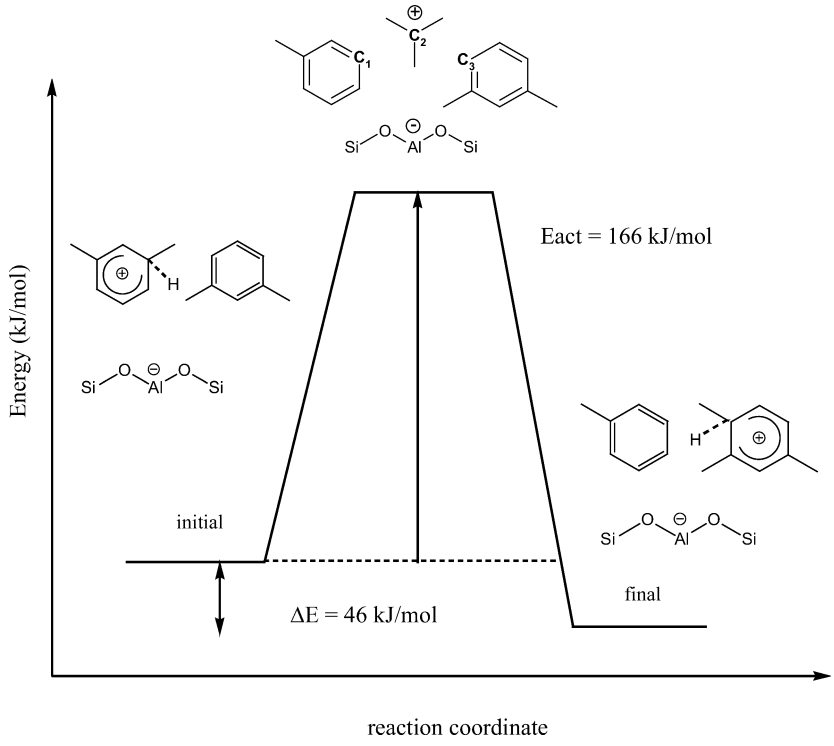

Fig. 3. Reaction energy diagram for the disproportionation reaction via a methyl shift in ZSM-22.

12-MR axis. Since the difference for the activation energies between TON and MOR is around 14 kJ/mol, we conclude that the (de)stabilization effect of the anionic lattice on the cationic transition state plays only a minor role. Whatever the channel size, and whatever the number of methyl groups at the molecule, the large energy barriers found in TON and MOR are due to the intrinsic unstable character of the methyl ion. As a consequence, the barriers involved in the formation of the three different TMB isomers are expected to exhibit rather small energy differences, which hence cannot help to explain the high selectivities found experimentally for the 1,2,4-TMB products in 10- or 12-MR pores [9–11].

3.2. Formation of the benzylic carbocation in TON

The alternative pathway occurs via the formation of a benzylic carbocation followed by the formation of a trimethyldiphenylmethane (protonated or not). The complete mechanism is depicted in Fig. 4. The first step (described in this section) occurs via the protonation of one xylene at the terminal C2 carbon atom of the methyl group. In order to avoid a fivefold coordinated carbon, one methyl C2–H bond breaks and leads to the first intermediate configuration, viz. a methyl-benzylic cation interacting weakly with the second neutral xylene. Additionally, this reaction step creates molecular hydrogen, diffusing out of the channel. Inversely, it is known experimentally that hydrogen inhibits the disproportionation reaction of toluene, which can be explained by this mechanism [30]. The formation of the methyl-benzylic cation is assumed to be the rate-limiting step. In TON, the reactant configuration exhibits two xylenes with one weakly adsorbed at the acidic proton of the zeolite (Fig. 4, step 1). The adsorption geometry is best characterized by a η_2-like adsorption mode, with two nearly equal distances between the zeolitic proton and the carbon atoms of the molecule (about 2.2 Å). The main reaction step for the formation of the benzylic carbocation is the protonation at the C2 carbon atom of one methyl group (Fig. 5). Simultaneous with the transfer of the proton, one C2–H bond of the methyl group breaks heterolytically. Subsequently, due to the recombination between the zeolitic proton and the hydride ion originating from the methyl group of xylene, molecular hydrogen is formed as a by-product. The transition state geometry is shown in Fig. 5. The former hydroxyl bond length is broken (O_{zeo}–H distance around 2.66 Å), as well as the C2–H bond of the xylene's methyl group (distance about 1.36 Å). The formation of H_2 is nearly complete as indicated by the H–H bond distance, close to that of molecular hydrogen (0.86 Å). Concerning the geometrical distortions of the reacting xylene molecule, the C2–C1 bond between the methyl group and the aromatic ring is strongly increased up to 1.47 Å, and an asymmetric distortion pattern is found for the two remaining C2–H distances of the former CH_3 group (1.10 vs 0.84 Å). Within the products, three molecules are present, i.e., a benzylic carbocation (primary carbenium ion), a neutral xylene, and molecular H_2. The hybridization of the C2 carbon atom changes to sp^2 and the C1–C2 bond length decreases to 1.37 Å. Due to the sp^2 hybridization, both hydrogen atoms are relaxing back into the plane of the ring with C1–C2–H angles around 121°. At

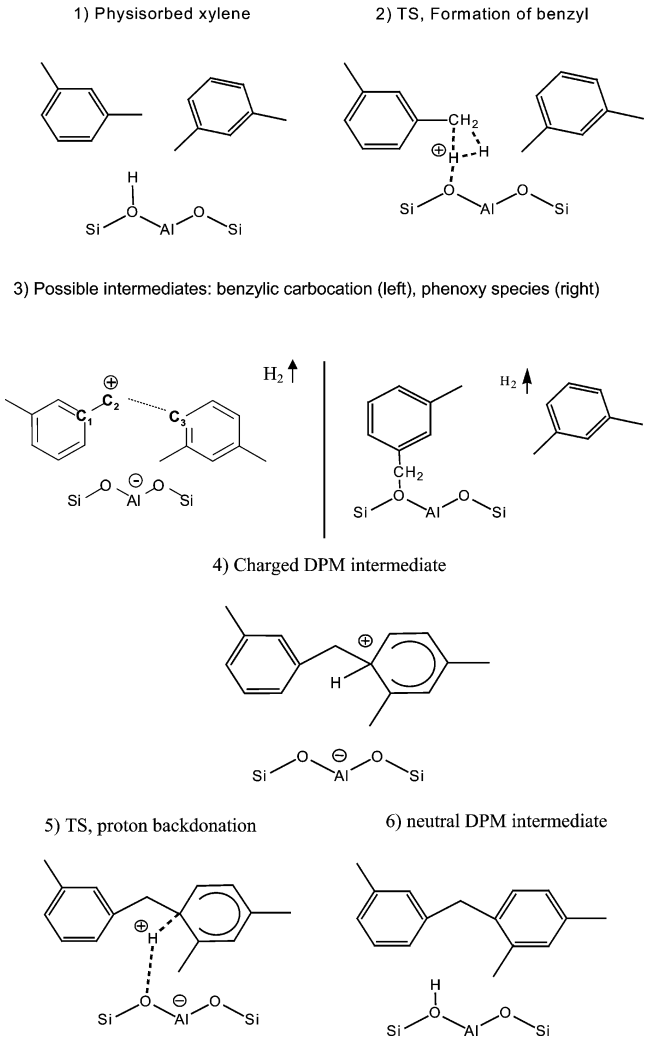

Fig. 4. Reaction mechanism of xylene disproportionation catalyzed by acidic zeolites via formation of the 2,4-dimethyl-1-(3-methylbenzyl)benzene intermediate.

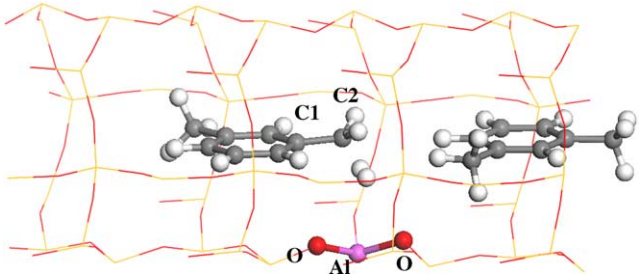

Fig. 5. Transition state geometry for the formation of a benzylic carbocation in ZSM-22 with proton transfer from the zeolite acid site.

this stage, it is important to underline again that in the case of TON (or more generally in 10-MR zeolites) the product configuration as benzyloxy species (see Fig. 4, step 3) is suppressed due to the strong electrostatic repulsion between the molecule and the zeolite lattice. We will come back to this point in the case of MOR.

As shown by the reaction energy diagram in Fig. 6, the barrier is evaluated at 212 kJ/mol, with respect to the reactant configuration (neutral physisorbed xylene molecule). As expected, the formation of a benzylic carbocation is an endothermic reaction; however, the energy difference between reactant and product is about 87 kJ/mol. The large value for the activation energy must be attributed to the breaking of a strong covalent C2–H single bond of the methyl group catalyzed by the acidic proton. Consequently, the value for this barrier only weakly depends on the pore-size radius of the zeolite. Indeed, Rozanska et al. [12] found a very similar activation energy of 221 kJ/mol for the formation of a benzyloxy intermediate in mordenite achieved by the same reaction step.

At this stage, the activation energy calculated for this initial step must be compared with the rate-limiting step of the transalkylation reaction mediated via a methyl shift. Since the barrier for the latter pathway is smaller by 46 kJ/mol, we might conclude that the benzylic carbocation formation would never be catalyzed by a Brønsted acid site. However, we suggest that this initiation step takes place at specific active centers (defect sites, EFAL, etc.). It will be shown in the next section that the further formation of the benzylic carbocation (during the catalytic cycle) can be achieved by a hydride shift between a charged TMB and xylene.

3.3. Formation of the DPM intermediates in TON

The recombination reaction between the methyl-benzylic cation and the second xylene molecule results in the formation of a charged trimethyldiphenylmethane intermediate (see Fig. 4, steps 3 and 4). It is important to underline the different aromatic properties between a methyl-benzylic cation, preserving the aromaticity and a benzenium-like carbocation, which loses partially its aromatic character.

The configuration of the reactants shows that the benzylic carbocation is stabilized by a weak interaction with the neighboring xylene (C2–C3 distance about 2.56 Å). Due to this interaction, the hydrogen atom (Ht) of the former neutral xylene, now attached to the C3 carbon atom involved in the newly formed C2–C3 bond, tilts out by 6° with respect to the aromatic plane. This Ht atom will be transferred subsequently to the oxygen of the zeolite framework. For this recombination step, the total energy decreases linearly as the C2–C3 distance decreases. As soon as the two molecules approach each other they recombine spontaneously, yielding the trimethyldiphenylmethane (called DPM) cation, as depicted in Fig. 7a. The barrier for this step is hence expected to be very small. It should be noted that this benzenium ion preserves its aromaticity. The newly created C2–C3 bond is weaker (1.60 Å) than the adjacent single C1–C2 bond (1.51 Å). The C3–Ht bond elongates to 1.19 Å, and the Ht atom tilts strongly out of plane. The Ht–O_{zeo} distance is about 2.32 Å. Due to the strong steric influence of the small 10-MR channel, the protonated DPM is strongly distorted, as compared to the gas-phase geome-

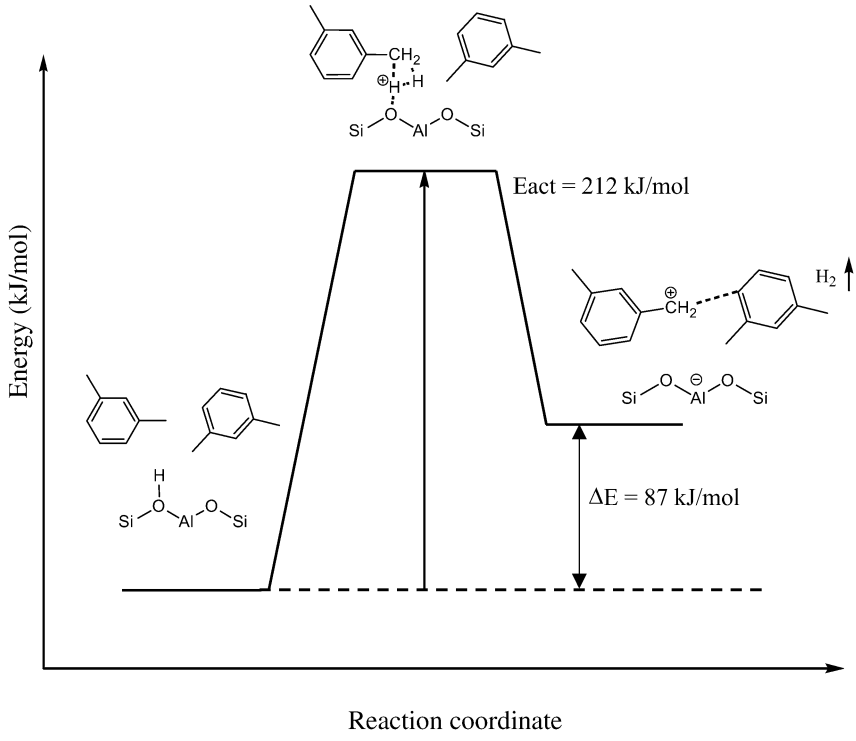

Fig. 6. Reaction energy diagram for the formation of a benzylic carbocation in ZSM-22.

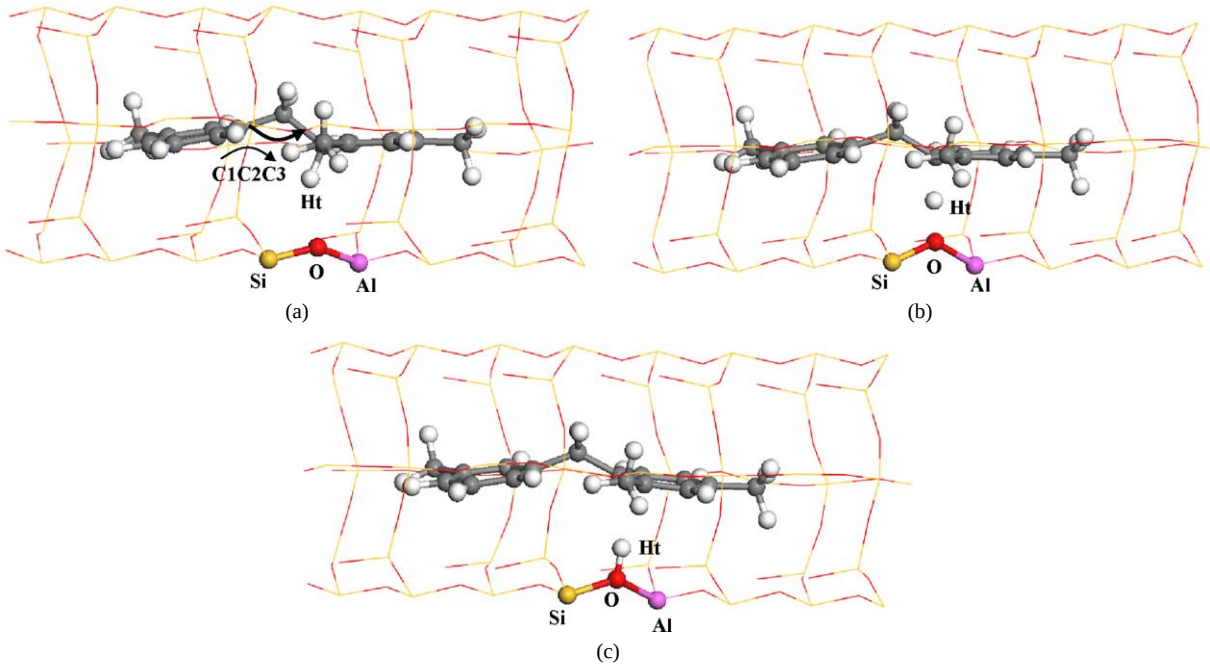

Fig. 7. Initial (a), transition state (b), and product configuration (c) for the formation step of a trimethyldiphenylmethane intermediate (2,4-DPM) in ZSM-22.

try. More precisely, the main geometrical change concerns the C1C2C3 angle (Fig. 7a) characterizing the opening of the two aromatic planes. For the protonated DPM optimized in the gas phase this angle is about 114°, whereas for the one adsorbed in TON, this angle increases by approximately 17° leading to a rather flat geometry of the molecule.

To proceed further with the reaction mechanism, the next intermediate configuration is formed via a proton backtransfer from the DPM to a zeolitic oxygen atom (Fig. 4, steps 5 and 6) leading to the neutral adsorbed DPM. The corresponding transition state structure is displayed in Fig. 7b; the Ht proton is located in an intermediate position between the C3 atom of the DPM (1.36 Å) and the oxygen atom of

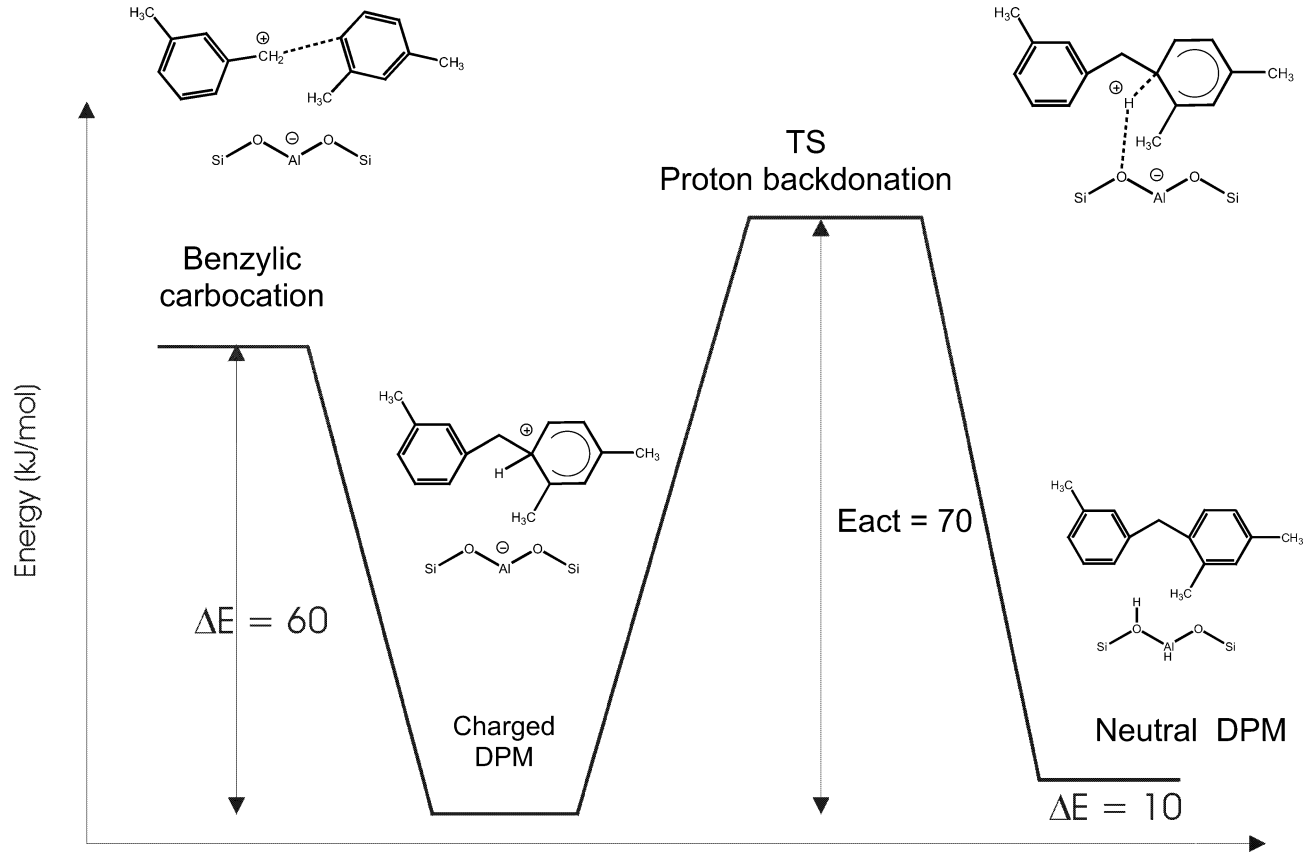

Fig. 8. Reaction energy diagram for the formation of a DPM intermediate in ZSM-22.

the framework (1.44 Å). Concerning the DPM, the C2–C3 distance decreases from 1.60 to 1.57 Å, together with the neighboring C–C bond lengths in the aromatic ring (around 1.43 Å). The DPM configuration (see Fig. 7c) corresponds to a η_2-like adsorbed DPM on the Brønsted site of TON. The two smallest distances between the acidic proton and the DPM carbon atoms are around 2.23 Å; the hydroxyl bond length is about 1.02 Å. The steric constraints acting on the molecule are still large, as indicated by the large and unchanged value of the C1C2C3 angle with respect to the protonated species.

The corresponding reaction energy diagram is shown in Fig. 8. Comparing the stability of the protonated DPM with the benzylic carbocation interacting with xylene, the former one is stabilized by 60 kJ/mol. The activation energy for the proton backdonation is around 70 kJ/mol. Moreover, the final configuration of the adsorbed DPM is by 10 kJ/mol less stable than the charged species. This is a surprising result since normally in zeolite frameworks, charged species (transition states or stable intermediates) are energetically much less stable than the corresponding neutral complex [29]. In the case of TON, the situation is obviously the reverse. The attractive Coulomb interaction is much too small to account for the unstable character of the charged hydrocarbon molecules (which is especially the case for primary and secondary carbenium ions). Actually, there is still a debate in the literature whether these ionic configurations are thermodynamically stable or exist only as transition states on the potential energy surface. Based on these considerations, it was surprising for us to see that within the small pores of TON the neutral physisorbed configuration is less stable than the charged one (which is not the case for MOR). To our mind, the only explanation is the large steric constraints in TON acting on the molecule. Moreover, one should also keep in mind that the disproportionation reaction in TON is proceeding in a high-energy regime in a sense that the "adsorption energy" of each configuration along the minimum energy path remains endothermic (we will discuss in more details this point in Section 3.5).

In order to fully achieve the disproportionation reaction, an acidic proton activates the DPM at the carbon atom on the second aromatic cycle. Subsequently, the DPM dissociates via a C1–C2 cleavage to one neutral toluene, and one charged trimethylbenzene (dimethyl-benzylic carbocation). At this stage, and as suggested in previous publications [5] the creation of a new methyl-benzylic carbocation ($C_8H_9^+$) can be catalyzed by this charged TMB^+:

$$C_8H_{10} + TMB^+ \rightarrow C_8H_9^+ + TMB. \quad (1)$$

Reaction (1) occurs via a hydride transfer from the neutral compound to the charged species. Since the disproportionation reaction is a cyclic reaction, the continuation of the cycle can be ensured by the TMB carbocation itself. For the proposed reaction an activation energy of 20 kJ/mol is

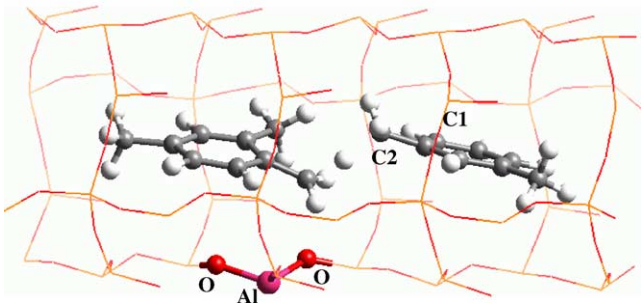

Fig. 9. Transition state geometry for the formation of a benzylic carbocation in ZSM-22 via a hydride shift from neutral xylene to charged TMB.

found, and the product and reactant configuration are very close in energy ($\Delta E \sim 5$ kJ/mol). For the TS geometry (see Fig. 9), the hydride ion is located in-between the two molecules (C–H distances around 1.35 Å). Subsequently, a neutral TMB is formed, simultaneously with a benzylic carbocation (methyl-benzyl ion). Such an alternative lower energy pathway allows this mechanism to be less energy demanding and more easily conceived, assuming that the formation of a benzylic species must be initiated once, probably at a defect site (as proposed in Section 3.2).

3.4. Formation of the DPM intermediates in MOR

We did not calculate transition states in MOR; however, from a comparison of the intermediate configurations and energies, significant insights are obtained for the reaction mechanisms and effect of pore sizes. It is interesting to compare the geometry and energy of the most relevant intermediate configurations along the minimum energy path of the *m*-xylene disproportionation reaction catalyzed by acidic mordenite. One difference between MOR and TON originates from the possible formation of benzyloxy species instead of the free charged benzylic carbenium (see Fig. 4, step 3), which is sterically hindered in 10-MR channel zeolites. The final optimized configuration of a surface benzyloxy for *m*-xylene is shown in Fig. 10a. However, it is important to note that only one type of aluminum site, facing the 8-MR side pockets, allows this formation, since the upper methyl group points inside the 8-MR side pockets. For other aluminum sites along the main 12-MR, as in the case of TON, the benzyloxy formation is not possible. The protonated DPM configuration and the final adsorbed DPM in H-MOR are displayed in Figs. 10b and 10c. It is seen that the steric constraints in the 12-MR channel are far less pronounced than in TON; e.g., the molecular C1C2C3 angle

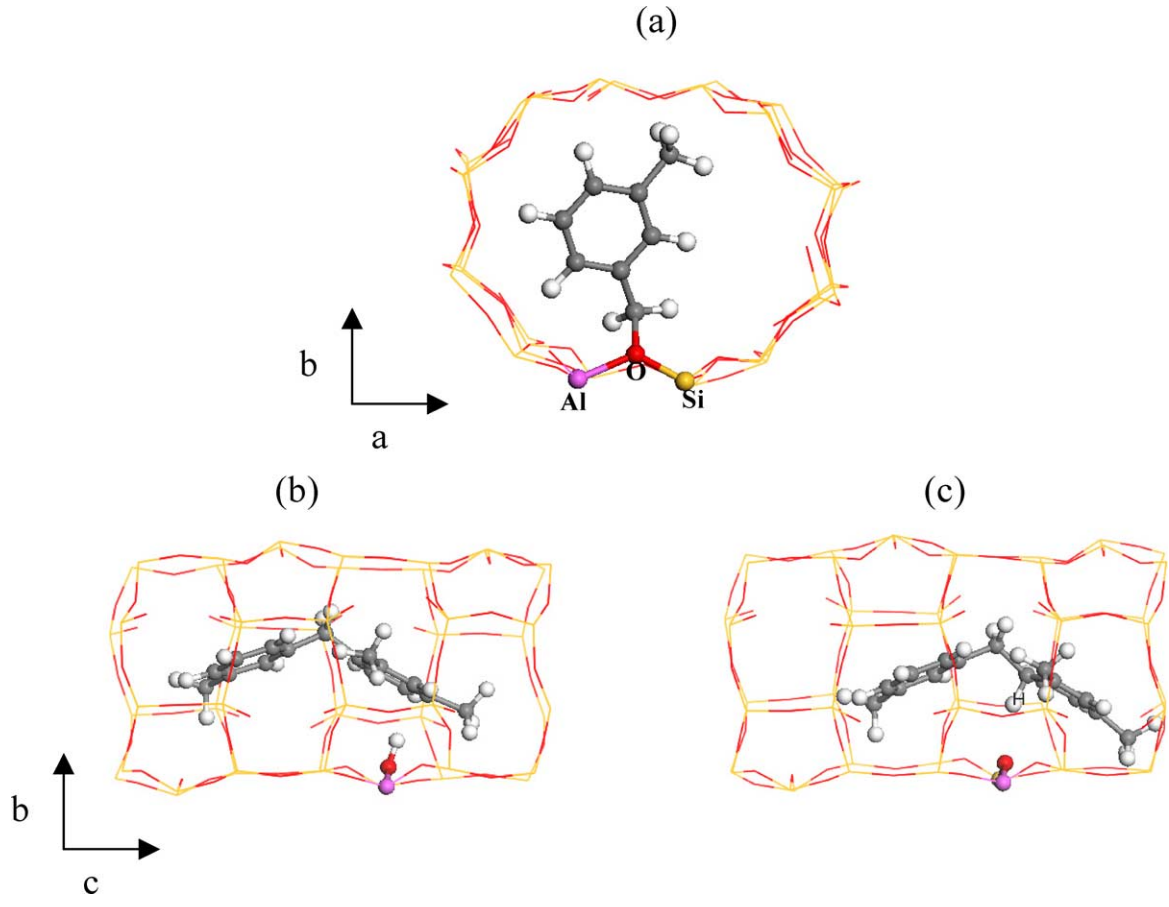

Fig. 10. Geometries of the intermediate configurations for the benzyloxy compound (a), the neutral DPM (b), and charged DPM molecule (c) in mordenite.

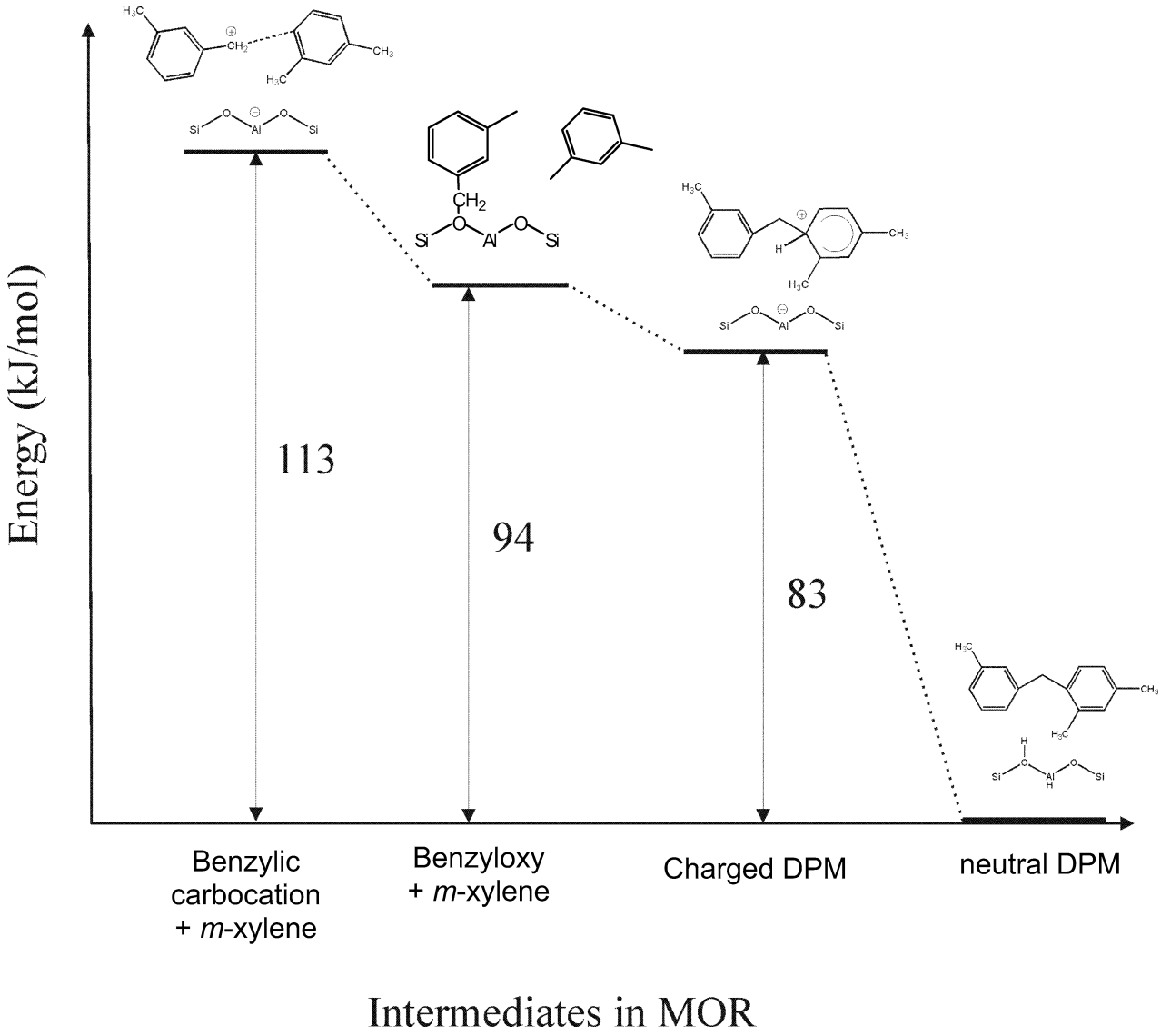

Fig. 11. Energetic stability of the various intermediate configurations of *m*-xylene disproportionation in mordenite (energies in kJ/mol with respect to the most stable intermediate, i.e., neutral DPM).

increases only by 6°, as compared with the gas-phase value. As in TON, this angle is similar for the charged and neutral DPM. At the same time, the distance between the acidic proton and the oxygen atom of the framework is around 2.14 Å, indicating a similar amount for the Coulomb interaction between the acidic proton and the aromatic ring. For the charged DPM, as in TON, the C3–Ht distance is around 1.15 Å (see Fig. 10c).

The energetic stability of the intermediate configurations is displayed in Fig. 11. The benzyloxy + *m*-xylene species are only by 19 kJ/mol more stable than the benzylic carbocation + *m*-xylene and about 11 kJ/mol less stable than the charged DPM. This implies that even if the specific position chosen for the aluminum atom facilitates the benzyloxy formation, this species remains energetically unfavorable with respect to the charged DPM. In any case, following the reaction path, the charged DPM configuration must be formed and the direct recombination of the benzylic carbocation leading to the charged DPM without creating the benzyloxy species is thermodymically favored, since a further transition state, corresponding to the breaking of the benzyloxy covalent C–O bond, can be avoided. For the disproportionation reaction of toluene and benzene in mordenite, Rozanska et al. [12] found that the charged DPM is less stable than the benzyloxy + toluene species by about 33 kJ/mol. Thus, the presence of one additional methyl group on the benzyloxy implies that due to larger sterical constraints acting on the molecule, the energetic ordering is the reverse.

A further important concern is the relative energy of the charged and neutral DPM species. In the case of MOR, as expected, the adsorbed neutral configuration is more stable (by 83 kJ/mol) with respect to the charged compound (see Fig. 11). This corroborates our former argument that in

TON, the steric constraints are mainly responsible for the leveling effect on energies of charged and neutral DPMs. Simultaneously, the benzylic carbocation + *m*-xylene compound is by 113 kJ/mol less stable than the final neutral DPM intermediate, whereas for TON, the energy difference was 50 kJ/mol only (Fig. 8). This is again an insight revealing how the sterical hindrances modify the energy profile.

3.5. Selectivity in TON and MOR

We have studied so far the reaction path implying the formation of the 2,4-dimethyl-1-(3-methylbenzyl)benzene, called 2,4-DPM, and yielding 1,2,4-TMB. To further investigate the experimental selectivities observed in isomerization/disproportionation and TMB by-products, it is mandatory to extend the investigation to all possible isomers of the trimethyldiphenylmethane intermediates. As this would imply a study of about 50 isomers, we have decided to focus on the disproportionation reaction involving two xylenes, with at least one of them the *meta*-isomer. Ten different DPM-like intermediates only are formed, leading either to 1,2,4-TMB or 1,2,3-TMB or 1,3,5-TMB, simultaneously with one toluene molecule. All these possible isomers are summarized in Fig. 12. One notes that there exists only one DPM-like isomer (viz. the 3,5-dimethyl-1-(3-methylbenzyl)benzene) leading to the final 1,3,5-TMB molecule, while three different DPMs yield 1,2,3-TMB, and six DPM intermediates yield 1,2,4-TMB. It must be noted that the 2,3-DPM and the 5,6-DPM are actually conformers. This is also the case for the 2,4-DPM and 4,6-DPM, as well as for the 3,4- and 4,5-DPM, and for the 2,5- and 3,6-DPM. We decided to simulate separately these conformers, because in their adsorbed states, two conformers may lead to different potential energy surfaces due to the methyl group orientations with respect to the void space available in the framework. In the gas phase, the relative energy stability of the 10 isomers is given by the ΔE_{gas} values in Table 1. The largest energy difference of about 23 kJ/mol is found between the 2,6- and the 4,5-DPM; the latter one also exhibits

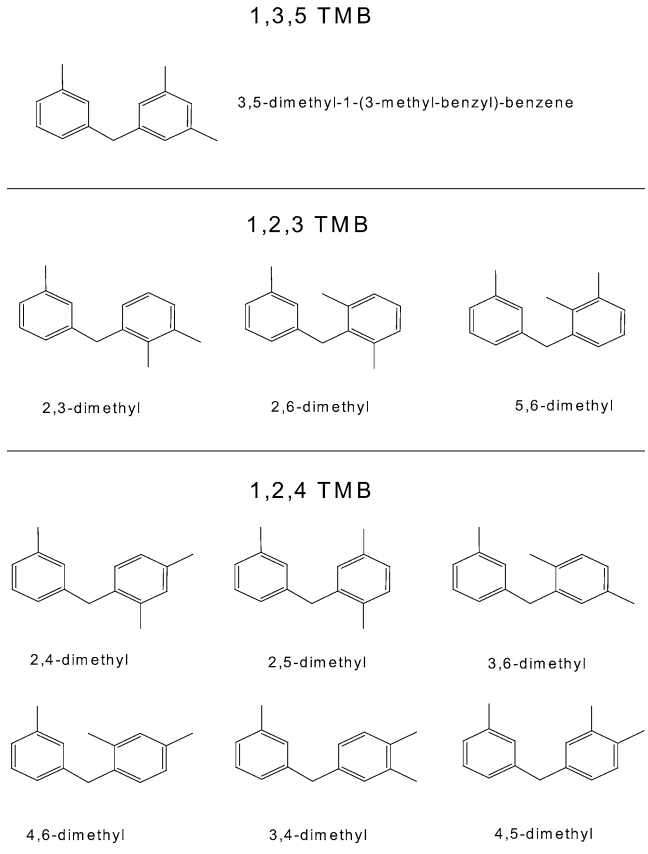

Fig. 12. Various trimethyldiphenylmethane isomers and conformers formed during the disproportionation reaction between a *m*-xylene and a second *p*/*o*/*m*-xylene molecule and grouped according to the final TMB isomer.

the lowest energy among all DPMs. The energetic ordering is correlated with the number of short H–H distances either between hydrogen atoms of neighboring methyl groups or between H atoms of the central sp^3 C2 carbon atom and hydrogen atoms of adjacent methyl groups. For instance, DPMs yielding 1,2,3-TMB are all less stable, whereas the 3,5-DPM is energetically strongly disfavored.

From a statistical point of view, the high selectivity for 1,2,4-TMB might be expected. However, this approach

Table 1
Adsorption energies and geometrical parameters of the various DPM intermediates adsorbed in acidic TON

TMB product	DPM type	ΔE_{gas} (kJ/mol)	$E_{ads,DFT}$ (kJ/mol)	$\Delta E_{ads,DFT}$ (kJ/mol)	E_{vdW} (kJ/mol)	E_{ads} (kJ/mol)	ΔE_{ads} (kJ/mol)	ΔC1C2C3 (deg)	*N*
1,3,5	3,5-DPM	1.5	243.2	138.5	−126.1	117.2	179.1	14.4	17 (3/4)
1,2,3	2,3-DPM	14.1	219.3	114.6	−128.7	90.6	152.5	16.4	16 (3/3)
	2,6-DPM	22.9	195.9	91.2	−139.0	56.9	118.8	14.9	11 (2/2)
	5,6-DPM	8.8	182.9	78.2	−127.1	55.8	117.7	10.0	12 (3/0)
1,2,4	2,4-DPM	7.9	147.3	42.6	−158.1	−10.7	51.1	17.7	12 (0/3)
	4,6-DPM	8.9	180.6	75.9	−123.7	56.9	118.8	12.6	14 (3/1)
	2,5-DPM	11.5	181.3	76.6	−148.7	32.6	94.5	17.9	13 (0/4)
	3,6-DPM	1.5	209.4	104.7	−131.2	78.2	140.1	7.5	13 (1/3)
	3,4-DPM	0.8	171.1	66.4	−138.4	32.7	94.6	11.2	15 (0/3)
	4,5-DPM	0	104.7	0	−166.6	−61.9	0	13.4	10 (0/0)

N stands for the number of close contacts (O_{zeo}–H_{mol} distances smaller than 2.5 Å) with the zeolite framework: the values for the two methyl groups branched on the same aromatic ring are bracketed. ΔX values represent variations with respect to the most stable isomer.

would assume that all adsorbed DPMs are thermodynamically equally possible, which is not a priori true. Indeed, different sterical constraints acting on the various DPM isomers may modify the thermodynamic stability ranking and displace a purely statistical distribution. So far, it was believed that DPM exists only as a transient intermediate along the minimum energy path leading to restricted transition state selectivity. However, as we have shown in this study, the various DPM isomers (protonated or not) are stable intermediates, which is also in agreement with a recent theoretical study of Clark et al. [13]. Since a transition state search along the pathways involving all DPM isomers in TON and MOR is beyond the available computational resources, our analysis focuses on the adsorption step of the ten DPM-like intermediates in both zeolites.

3.5.1. Selectivity in TON

The results for TON are reported in Table 1. All geometrical parameters correspond to the neutral physisorbed DPM in acidic TON. The $E_{\mathrm{ads,DFT}}$ values correspond to adsorption energies as calculated within the DFT approach and after full geometry optimization. $\Delta E_{\mathrm{ads,DFT}}$ stands for the relative energy difference with respect to the most stable DPM isomer. As observed in Table 1, DFT calculated adsorption energies are endothermic with a very large dispersion according to the various isomers. As a very first remark, it can be underlined that the relative and absolute values of $\Delta E_{\mathrm{ads,DFT}}$ differ significantly from those of ΔE_{gas}, revealing the key role of the framework. The most stable configuration corresponds to the 4,5-DPM isomer, and the least stable corresponding to the 3,5-DPM lies 138 kJ/mol higher in energy. Moreover, we found that the five most stable configurations (viz. 4,5; 2,4; 3,4; 4,6; and 2,5) lead to the 1,2,4-TMB isomer.

The adsorption energies reported so far are based exclusively on DFT calculations, and as we noted previously, this methodology does not take dispersive interactions into account. Dispersive forces, however, dominate the interaction between an aromatic and a zeolite. It is thus required to correct the DFT values for vdW contributions (for technical details, see Methods). The corresponding energies, E_{vdW}, are reported in Table 1, together with the total corrected, E_{ads}. Obviously, dispersive contributions are exothermic and exhibit a scattering of about 43 kJ/mol, significantly smaller than that of DFT contributions. In particular, the order of adsorption energies of the two most and three least stable DPMs in TON remains unchanged after including vdW contributions. This is due to the fact that the differences in energy are mainly governed by electrostatic contributions rather than dispersive forces. However, the latter cannot be neglected. With respect to the final TMB products, the adsorption energies are ordered as follows: $E_{\mathrm{ads}}(1,3,5) > E_{\mathrm{ads}}(1,2,3) > E_{\mathrm{ads}}(1,2,4)$. According to the adsorption energies including vdW corrections, one notes that the two DPM configurations, which exhibit an exothermic adsorption, lead to the observed 1,2,4-TMB product. All remaining adsorbed DPMs exhibit endothermic adsorption energies, and the formation of 1,2,3- and 1,3,5-TMB is thus strongly disfavored. The vdW contributions allow one to obtain reliable absolute values of adsorption energies in order to distinguish between endothermic and exothermic regimes. Furthermore, the absolute values are crucial for a consistent quantitative comparison of different frameworks and pore sizes. In any case, these levels of the calculated adsorption energies enable an explanation of why the experimental selectivities observed among the various TMB isomers are strongly pronounced (almost exclusively) in favor of 1,2,4-TMB within 10-MR zeolites [9–11]. The highly endothermic adsorption energies found for the DPM-like intermediates leading to 1,3,5- and 1,2,3-TMB thus give a quantitative argument of these experimental observations.

To better understand the nature of the DPM zeolite interaction, it is worth decomposing the adsorption energy in various terms according to the deformation of the molecule as well as of the zeolite. The deformation energy for the zeolite is calculated as the difference between the total energy of the energy value of the zeolite framework after optimization with the adsorbate subtracted by the optimized zeolite structure (without adsorbate). For the DPM molecule, the deformation energy is the difference between the molecule configuration in the adsorbed state and the gas-phase state. For the 3,5-DPM (least stable intermediate), the framework deformation energy is equal to 58 kJ/mol, while for the molecule it is 62 kJ/mol. Hence, a global amount of 120 kJ/mol is paid for the deformation of the system upon adsorption. The remaining part of the adsorption energy (i.e., 123 kJ/mol) corresponds to the balance between the attractive part (electrostatic and hydrogen bond interactions) and the large repulsive part arising from Coulomb repulsion between the H atoms of the molecule and the framework atoms at short distances. Concerning the most stable intermediate, i.e., the 4,5-DPM, the deformation energies are significantly reduced: 48 kJ/mol for the molecule and 15 kJ/mol for the framework. In both cases, about half of the value of the endothermic adsorption energy results from the deformations of the system. Besides, it must be stressed that the framework deformation energy is more sensitive to the DPM type than the molecule deformation energy itself.

The destabilization energy is correlated with the amount of steric constraints acting on the adsorbates. These constraints can be expressed by the number of closest contacts (smaller than 2.5 Å, according to the chosen criterium) between the hydrogen atoms of the adsorbed intermediate and the oxygen atoms of the framework, as summarized in Table 1. For the least stable configuration (3,5-DPM), the number of closest contacts is the highest, whereas the most stable configuration (4,5-DPM) exhibits the smallest number of such distances. Additionally, one can note that the destabilization energy is found to be the highest when the contacts are located on the two methyl groups belonging to the same DPM's aromatic ring. In this case, the aromaticity of the ring is strongly perturbed, implying the highest energy destabilization. For the energetically least stable adsorption

mode (3,5-DPM), three short distances at one CH_3 group and four contacts at the other methyl group are present, whereas no such constraints are found for the most stable adsorption geometry. If one CH_3 group only is affected, the configuration is generally more stable (2,5-DPM versus 2,6-DPM). One relevant structural deformation of the adsorbed DPM molecule concerns the angle between the two aromatic planes, called C1C2C3 in Fig. 7a. These values with respect to the gas phase are reported in Table 1 for the different DPMs. However, it must be stressed that there is no direct correlation between the destabilization energies and the C1C2C3 angle deformation. If we compare the two extreme cases represented by the 3,5-DPM and the 4,5-DPM, the C1C2C3 angle differs by only 1°. This corroborates our aforementioned result, showing that the deformation energy of the molecule is less sensitive to the DPM than the framework deformation.

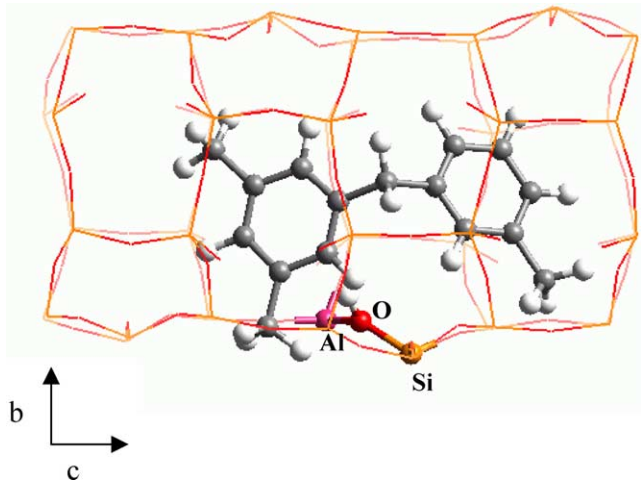

Fig. 13. Optimized adsorption geometry of 3,5-DPM in acidic mordenite with aromatic rings perpendicular to the *a* axis.

3.5.2. Selectivity in MOR

Although MOR is regarded as a zeolite exhibiting a one-dimensional channel system, due to the existence of 8-MR side pockets several possible adsorption modes for the DPM isomers exist. So far we have concentrated our analysis to an adsorption geometry, where the DPM molecule is adsorbed along the main 12-MR, with the planes of the two aromatic rings mostly perpendicular to the *b* axis (see Fig. 10b and 10c). However, due to the presence of side pockets, the DPM intermediate may also adsorb with the planes of the two aromatic rings perpendicular to the *a* axis, as represented in Fig. 13 for the 3,5-DPM. The investigation of such an adsorption geometry is motivated by the fact that the hydrogen atoms of the DPM methyl groups can point toward the 8-MR side pockets, which may significantly modify the DPM stability. In what follows, we will discuss the two possible adsorption modes in detail.

3.5.2.1. Adsorption with rings perpendicular to the b axis

This adsorption mode is the one already used in Section 3.4, for the 2,4-DPM formation mechanism. In this case, the Al4–O10(H) acid site is chosen as an active center. The adsorption energies for the different DPMs in H-MOR are reported in Table 2. First, one notes that the energy dispersion, $\Delta E_{\mathrm{ads,DFT}}$, as well as ΔE_{ads} (around 55 kJ/mol), is much less pronounced than in TON. After applying the vdW correction term, adsorption energies are all negative; i.e., the adsorption process becomes generally exothermic. The two most stable adsorption modes (3,4- and 2,4-DPM) indicate that the 1,2,4-TMB yield must be the highest. This can be clearly explained by the reduced number of close contacts as compared to the TON framework. This result is again in agreement with the experimental TMB product pattern observed in MOR where 70% in 1,2,4-TMB is found experimentally, as reported in [9–11]. Based on the calculated adsorption energies, the two isomers (1,2,3- and 1,3,5-TMB) can be formed, but they are thermodynamically less favored. As shown in Table 2, the deformation of the C1C2C3 angle is significantly smaller (4–7°) than in the TON framework. Furthermore, the differences in the destabilization energies are rather small.

Table 2
Adsorption energies and geometrical parameters of the various DPM intermediates adsorbed in acidic MOR with aromatic rings perpendicular to the *b* axis

TMB product	DPM type	$E_{\mathrm{ads,DFT}}$ (kJ/mol)	$\Delta E_{\mathrm{ads,DFT}}$ (kJ/mol)	E_{vdW} (kJ/mol)	E_{ads} (kJ/mol)	ΔE_{ads} (kJ/mol)	ΔC1C2C3 (deg)	*N*
1,3,5	3,5-DPM	56.4	55.7	−126.9	−70.5	52.1	5.1	9
1,2,3	2,3-DPM	25.6	25.0	−100.3	−74.6	47.9	6.2	11
	2,6-DPM	31.3	30.6	−130.1	−98.7	23.8	6.9	7
	5,6-DPM	27.3	26.6	−136.5	−109.2	13.3	3.3	6
1,2,4	2,4-DPM	19.6	18.9	−132.0	−112.4	10.1	6.4	7
	4,6-DPM	17.2	16.5	−126.1	−108.8	13.6	4.6	7
	2,5-DPM	51.1	50.5	−124.8	−73.6	48.9	6.5	7
	3,6-DPM	45.2	44.6	−126.2	−80.9	41.6	3.4	7
	3,4-DPM	0.6	0.0	−123.2	−122.6	0.0	5.4	8
	4,5-DPM	32.4	31.7	−70.8	−38.4	84.1	3.7	12

N stands for the number of close contacts with the zeolite framework. ΔX values represent variations with respect to the most stable isomer.

Table 3
Adsorption energies and geometrical parameters of the various DPM intermediates adsorbed in acidic MOR with aromatic rings perpendicular to the *a* axis

Final TMB	Adsorbed molecule	$E_{ads,DFT}$ (kJ/mol)	$\Delta E_{ads,DFT}$ (kJ/mol)	E_{vdW} (kJ/mol)	E_{ads} (kJ/mol)	ΔE_{ads} (kJ/mol)	ΔC1C2C3 (deg)	*N*
1,3,5	3,5-DPM	27.3	0.0	−121.6	−94.2	0.0	5.5	10
1,2,3	2,3-DPM	44.7	17.4	−106.5	−61.7	32.5	5.4	12
	2,6-DPM	180.2	152.8	−58.3	121.9	216.1	6.1	18
	5,6-DPM	137.6	110.3	−90.7	46.9	141.2	4.1	14
1,2,4	2,4-DPM	87.2	59.8	−96.0	−8.8	85.4	3.1	13
	4,6-DPM	69.2	41.9	−111.6	−42.3	51.9	4.7	10
	2,5-DPM	58.5	31.2	−105.3	−46.7	47.5	5.1	14
	3,6-DPM	131.7	104.3	−93.9	37.8	132.0	5.1	11
	3,4-DPM	79.8	52.5	−99.4	−19.5	74.7	4.5	11
	4,5-DPM	46.9	19.6	−119.1	−72.1	22.1	2.5	8

N stands for the number of close contacts with the zeolite framework. ΔX values represent variations with respect to the most stable isomer.

3.5.2.2. Adsorption with rings perpendicular to the a axis The Al2–O2(H) acid site leading to this different orientation of the adsorbed molecule is chosen in this case. Since the mean distances between the acidic proton and the carbon atoms of the aromatic ring are very close to those found in the previous adsorption mode (around 2.2 Å), we expect roughly the same amount of attractive electrostatic interactions.

The final optimized geometry of the physisorbed 3,5-DPM is shown in Fig. 13. One notes that two methyl groups of the aromatic rings are located inside two neighboring 8-MR side pockets. The adsorption energies of the DPMs in this configuration are compiled in Table 3. The 3,5-DPM yields the highest exothermic adsorption energy (about −94.2 kJ/mol). Compared to the previous adsorption mode, this geometry is favored by 24 kJ/mol. For all other DPMs, the adsorption yields higher values for the heat of adsorption. It is important to note the much larger differences of the adsorption energies (ΔE_{ads}) around 216 kJ/mol, than for the previous configuration (about 122 kJ/mol). Due to the small diameter of the side pocket (around 5.7 Å), methyl groups located in the close vicinity of the carbon atom connecting the two aromatic rings cannot find a stable position within the center of the 8-MR. This consequently leads to strong steric constraints and explains the high endothermic adsorption energies particularly for the 2,6- and 5,6-DPM.

As a consequence, the experimentally observed product pattern for the TMB isomers in MOR can only be understood if one takes into account the two previously described adsorption modes. As the relative distributions of Al4–O10(H) as well as Al2–O2(H) sites remain unknown, it is difficult to predict quantitatively the TMB pattern. Furthermore, a previous ab initio study [27] has shown that both sites exhibit very similar values in energy stability and OH-stretching frequencies. As a consequence, both sites are equally possible candidates for active centers, so that the following semiquantitative interpretation can be given. On the Al4–O10(H) site, the 1,2,4-TMB is clearly produced in the majority, resulting from the energetically favored corresponding DPM intermediates. According to our calculation, the next favored product is the 1,2,3-TMB, followed by the 1,3,5-TMB. However, since the 1,3,5-TMB is found experimentally as the second product [9–11], this means that the Al2–O2(H) site can also be an active center for the disproportionation reaction. By stabilizing the 3,5-DPM with its two methyl groups entering the 8-MR, the higher amount of 1,3,5-TMB can thus be explained.

3.5.2.3. Consequences for the (i/d) ratio Regarding the isomerization/disproportionation (i/d) ratio observed experimentally [9–11], it is known that in 10-MR frameworks such as ZSM-5 and ZSM-11, the selectivity is strongly in favor of the isomerization (i/d ratio greater than 20). On the contrary, in 12-MR zeolites such as MOR or MAZ, the (i/d) selectivity is inverted with a ratio lower than 2. At this stage of our calculations, this can be explained by the stability of the DPM-like intermediates, which are strongly destabilized in 10-MR ($-62 < E_{ads} < +117$ kJ/mol) in comparison to 12-MR ($-122 < E_{ads} < -70$ kJ/mol). To a certain extent, this may be a rational argument explaining why the disproportionation pathway is less favored in 10-MR. It must be underlined that the (i/d) selectivity cannot be explained within a methyl-shift mechanism, since the methyl cation energy is far less sensible to the pore size.

4. Conclusion

We have presented a detailed study of the pore size effects on the disproportionation reaction of *m*-xylene in 10- and 12-MR zeolites. Two reaction mechanisms have been investigated. An energy barrier of 166 kJ/mol is calculated for the rate-limiting step for the reaction occurring via a methyl shift in TON. This value, comparable to previously reported calculations in MOR, reveals that it depends weakly on the pore size. Hence, such a pathway fails to explain the different selectivities observed in 10-MR and 12-MR zeolites. The second reaction scheme is initiated by the formation of a benzylic carbocation. This initiation step cannot be catalyzed by an acidic proton because of the too high energy

barrier compared to the methyl shift (212 kJ/mol). This initiation step should actually take place at a defect site. However, the activation energy drops dramatically if a hydride transfer through a charged benzylic species is considered. As a consequence, the continuation step of the catalytic cycle is ensured by hydride shift occurring inside the pores and not at a defect site. A compound like a charged TMB already formed in the zeolite during the reaction may thus be used for this continuation step. Subsequently, the benzylic compound reacts with the second neutral xylene to form a DPM-like intermediate. The rate-limiting step of the reaction is found for the backdonation from the charged DPM to the zeolitic framework (around 70 kJ/mol).

The adsorption of 10 relevant DPM species formed during the *m*-xylene disproportionation has been studied. In 10-MR zeolites such as TON, the adsorption is generally found to be strongly endothermic except for some DPMs yielding the experimentally observed 1,2,4-TMB product. The formation of DPMs leading to the 1,3,5- or 1,2,3-TMB is suppressed due to large steric constraints. Additionally, we furnish an analysis of sterical constraints in terms of numbers of close contacts, correlating with the destabilization energy of the DPM. For MOR, the mechanism involving the DPM formation is more favored due to more exothermic adsorption energies of all DPM-like intermediate. A smaller amount of steric constraints is also evidenced by the small differences of the adsorption energies among the various DPMs. As in the MOR topology side pockets are present; the presence of two nonequivalent acid sites corresponding to two distinct adsorption configurations is mandatory for explaining the experimentally found product pattern. We hope that this approach based on a systematic adsorption energy calculation of DPMs can be applied for predicting selectivities in other zeolite topologies. In future work, we plan to apply it by investigating zeolites with interconnected 10-MR and 12-MR pores.

Acknowledgments

Fruitful discussions with Drs. Stéphane Morin and Theodorus de Bruin from IFP are greatly acknowledged. This work has also undertaken within the GDR Dynamique Quantique Appliquée à la Catalyse a joint project among IFP, CNRS, University of Vienna, and TOTAL.

References

[1] P.A. Jacobs, J.A. Martens, in: H. van Bekkum, E.M. Flaningen, J.C. Jansen (Eds.), Introduction to Zeolite Science and Practice, Elsevier, Amsterdam, 1991, p. 445.
[2] S.M. Csicsery, Zeolites 4 (1984) 202.
[3] T.C. Tsai, S.B. Liu, I. Wang, Appl. Catal. A 181 (1999) 255.
[4] F. Alario, M. Guisnet, in: G.J. Hutchings (Ed.), Zeolites for Cleaner Technologies, in: Catalytic Science Series, vol. 3, Imperial Collegie Press, London, 2002, p. 189.
[5] S. Morin, N.S. Gnep, M. Guisnet, J. Catal. 159 (1996) 296.
[6] A. Corma, E. Sastre, J. Catal. 129 (1991) 177.
[7] Y.S. Xiong, P.G. Rodewald, C.D. Chang, J. Am. Chem. Soc. 117 (1995) 9427.
[8] A. Corma, A. Chica, J.M. Guil, F.J. Llopis, G. Mabilon, J.A. Perdigon-Melon, S. Valencia, J. Catal. 189 (2000) 382.
[9] J.A. Martens, J. Perez-Pariente, E. Sastre, A. Corma, P.A. Jacobs, Appl. Catal. 45 (1988) 85.
[10] B. Adair, C.-Y. Chen, K.-T. Wan, M.E. Davis, Micropor. Mater. 7 (1996) 261.
[11] C.W. Jones, S.I. Zones, M.E. Davis, Appl. Catal. 181 (1999) 289.
[12] X. Rozanska, R.A. Van Santen, F. Hutschka, J. Phys. Chem. 106 (2002) 4652.
[13] L. Clark, M. Sierka, J. Sauer, J. Am. Chem. Soc. 125 (2003) 2136.
[14] G. Kresse, J. Hafner, Phys. Rev. B 48 (1993) 13115.
[15] G. Kresse, J. Hafner, Phys. Rev. B 49 (1994) 14251.
[16] J.P. Perdew, J.A. Chevary, S.H. Vosko, K.A. Jackson, M.R. Pedersen, D.J. Singh, C. Fiolhais, Phys. Rev. B 46 (1992) 6671.
[17] P. Blöchl, Phys. Rev. B 50 (1994) 17953.
[18] G. Kresse, D. Joubert, Phys. Rev. B 59 (1999) 1758.
[19] G. Mills, H. Jonsson, G.K. Schenter, Surf. Sci. 324 (1995) 305.
[20] J. Sauer, P. Ugliengo, E. Garrone, V.R. Saunders, Chem. Rev. 94 (1994) 2095.
[21] T. Demuth, L. Benco, J. Hafner, H. Toulhoat, F. Hutschka, J. Chem. Phys. 114 (2001) 3703.
[22] DISCOVER and COMPASS are delivered within the Cerius^2 interface commercialized by Accelrys Inc (for further informations see also the web site http://www.accelrys.com).
[23] H. Sun, J. Phys. Chem. 102 (1998) 7338.
[24] P. Raybaud, A. Patrigeon, H. Toulhoat, J. Catal. 197 (2001) 98.
[25] W.F. Hölderich, H. van Bekkum, in: H. van Bekkum, E.M. Flaningen, J.C. Jansen (Eds.), in: Introduction to Zeolite Science and Practice, vol. 58, Elsevier, Amsterdam, 1991, p. 631.
[26] G.T. Kokotailo, J.L. Schlenker, F.G. Dwyer, E.W. Valyocsik, Zeolites 5 (1985) 349.
[27] T. Demuth, J. Hafner, L. Benco, H. Toulhoat, J. Phys. Chem. 104 (2000) 4593.
[28] T. Demuth, X. Rozanska, L. Benco, J. Hafner, R.A. van Santen, H. Toulhoat, J. Catal. 214 (2003) 68.
[29] R.A. van Santen, G. Kramer, Chem. Rev. 95 (1995) 637.
[30] N.S. Gnep, M. Guisnet, J. Appl. Catal. 1 (1981) 329.